

## **Supporting Information**

### **Nanostructure Engineering and Performance Enhancement in**

### **Fe<sub>2</sub>O<sub>3</sub>-Dispersed Cu<sub>12</sub>Sb<sub>4</sub>S<sub>13</sub> Thermoelectric Composites with Earth-**

### **Abundant Elements**

Haihua Hu, Fu-Hua Sun, Jinfeng Dong, Hua-Lu Zhuang, Bowen Cai, Jun Pei, and

Jing-Feng Li\*

State Key Laboratory of New Ceramics and Fine Processing, School of Materials

Science and Engineering, Tsinghua University, Beijing 100084, P. R. China

\*Email: [jingfeng@mail.tsinghua.edu.cn](mailto:jingfeng@mail.tsinghua.edu.cn).

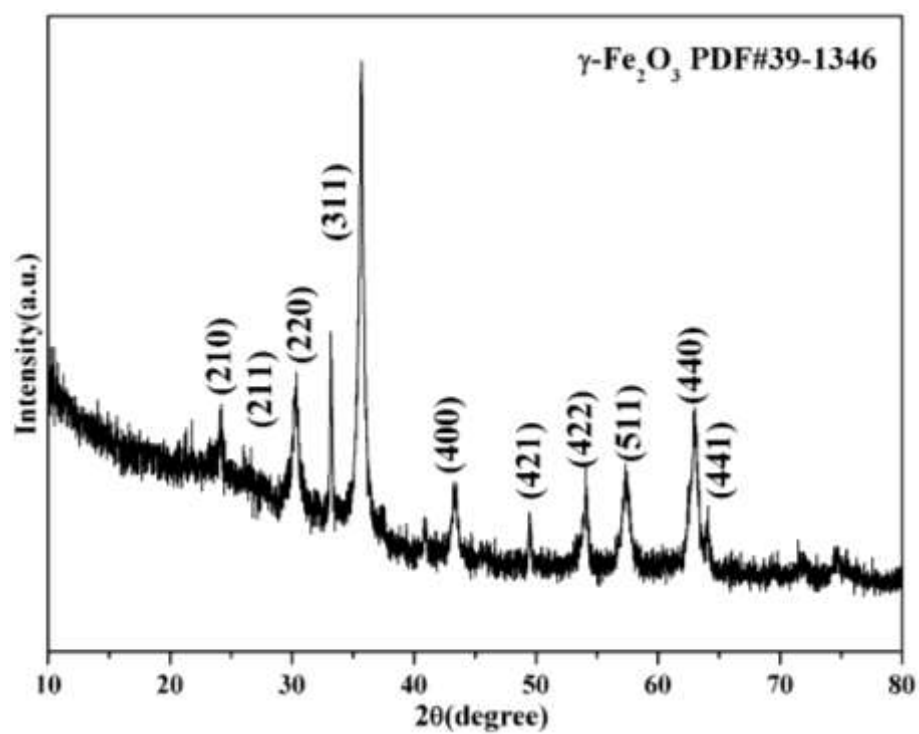


**Figure S1** XRD pattern of the magnetic  $\gamma\text{-Fe}_2\text{O}_3$  NPs.

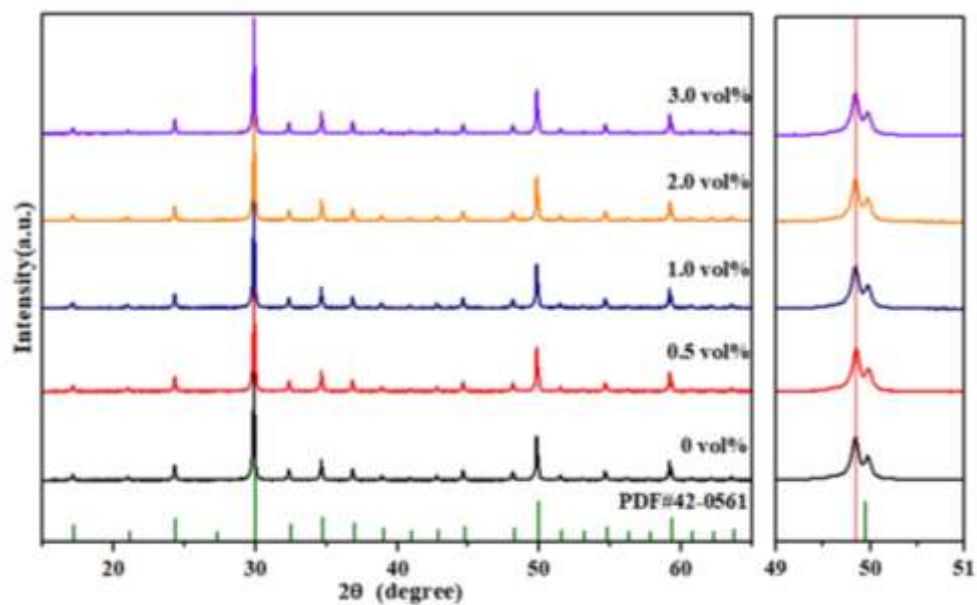


**Figure S2** XRD pattern of the obtained CNAS- $x$ Fe<sub>2</sub>O<sub>3</sub> ( $x = 0, 0.5, 1.0, 2.0$ , and  $3.0\%$ ) samples, along with the enlarged peaks between  $49$  and  $51^\circ$ .

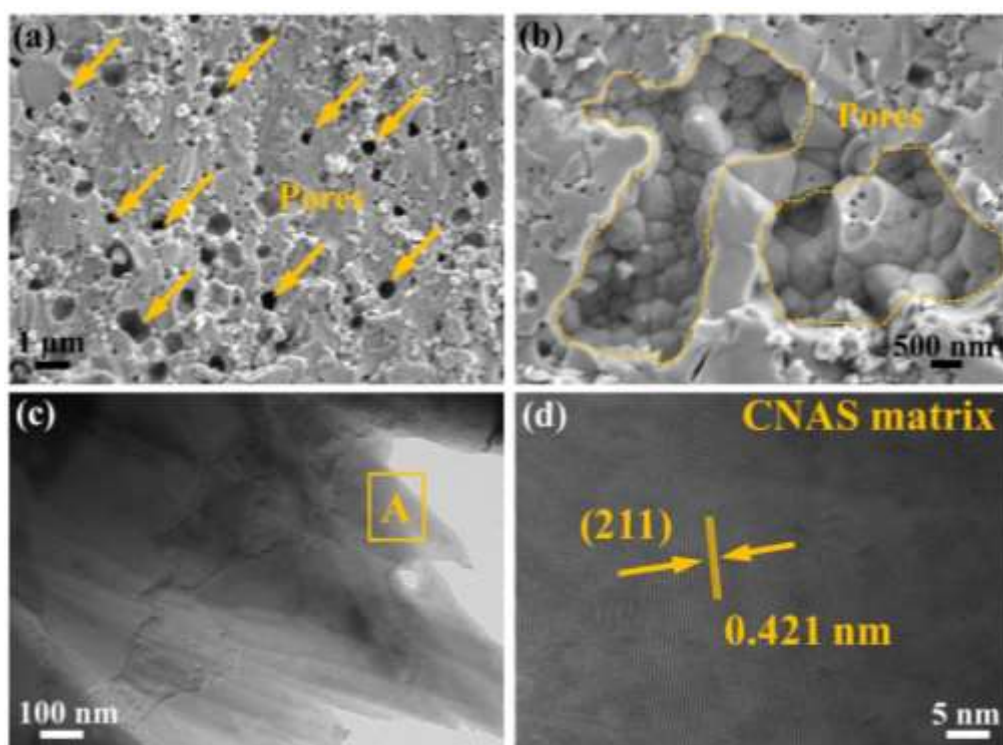


**Figure S3** (a-b) FESEM image of the CNAS matrix on the fractured surface, low-magnification TEM image (c) and HRTEM image (d) of the CNAS matrix.

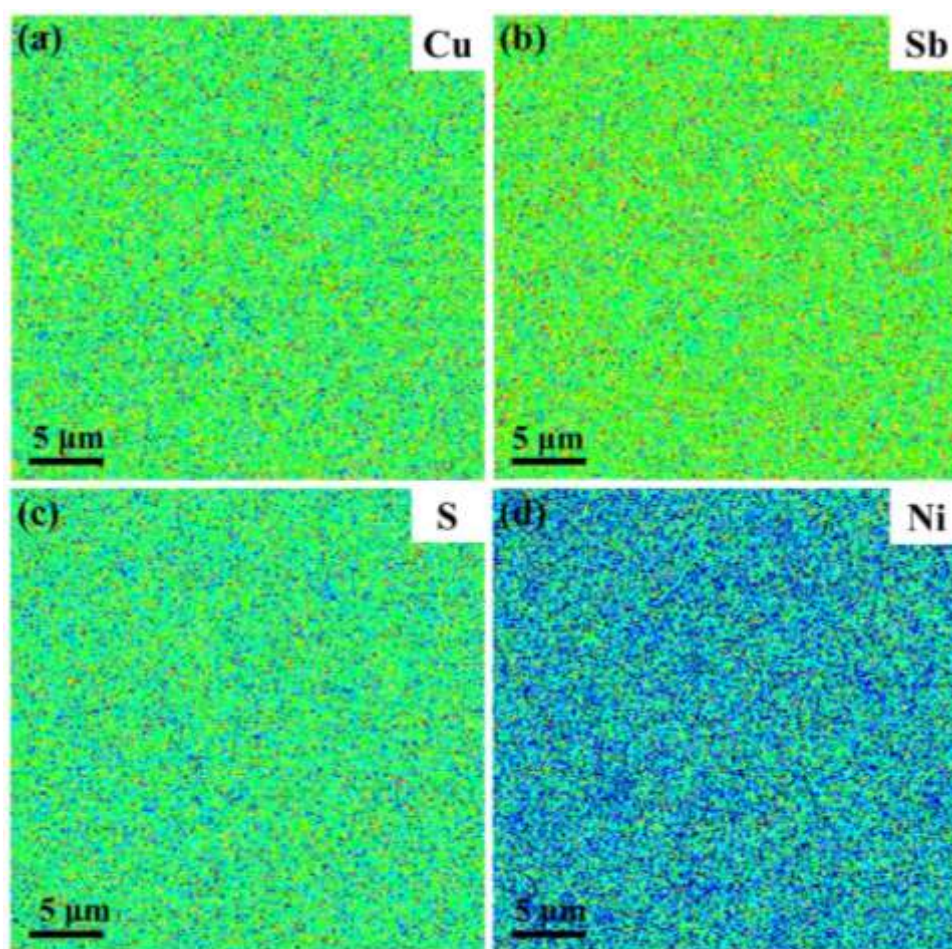


**Figure S4** EPMA mapping of (a) Cu, (b) Sb, (c) S, and (d) Ni taken from the matrix.

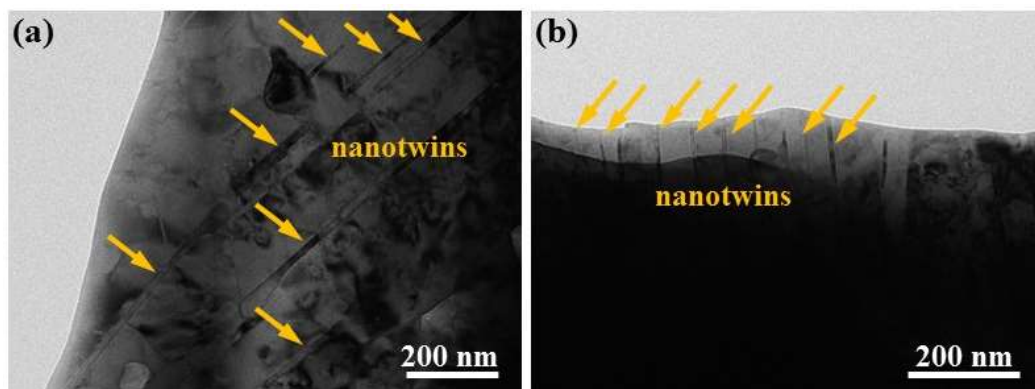


**Figure S5** (a-b) Low-magnification TEM pattern of the nanotwins in different areas of the CNAS-1.0%Fe<sub>2</sub>O<sub>3</sub> sample.

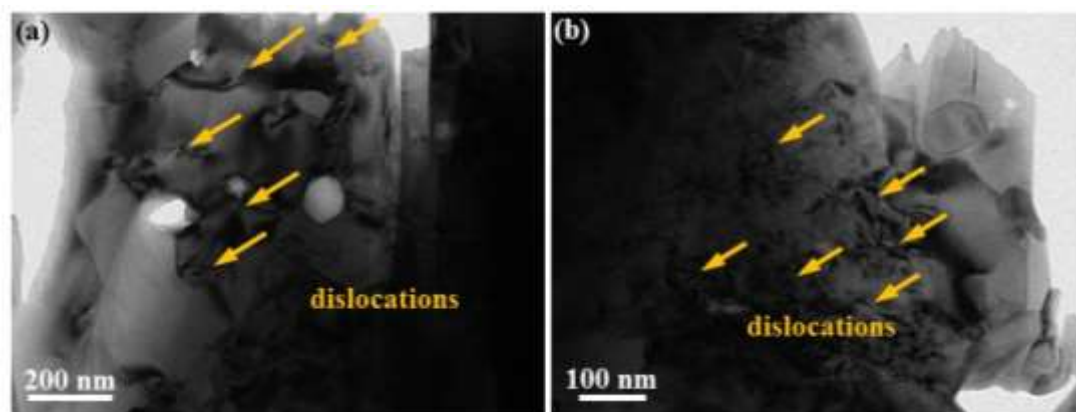


**Figure S6** (a-b) Low-magnification TEM pattern of the dislocations in the CNAS-1.0%Fe<sub>2</sub>O<sub>3</sub> sample;

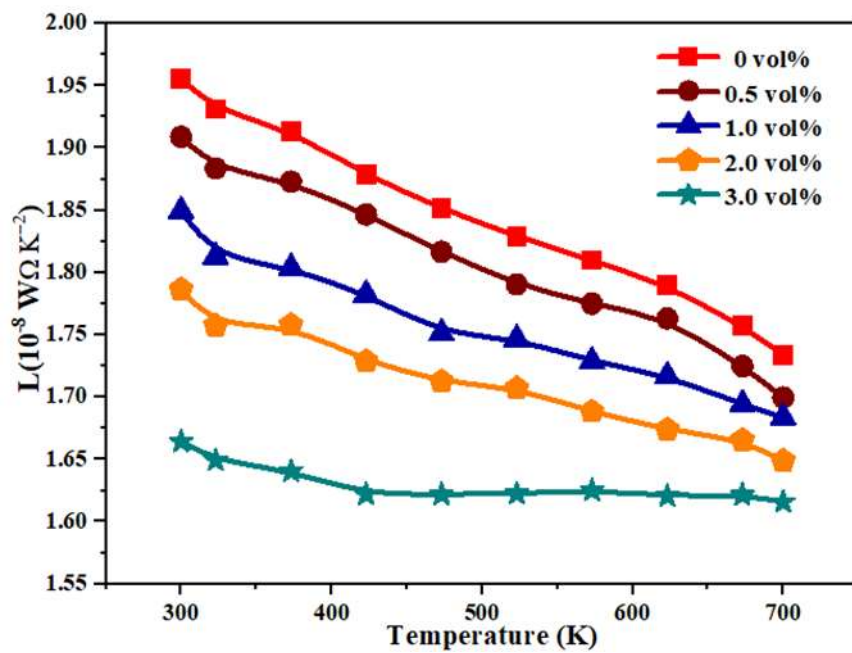


**Figure S7** The calculated Lorenz number for the CNAS- $x\text{Fe}_2\text{O}_3$  ( $x = 0, 0.5, 1.0, 2.0$ , and  $3.0\%$ ) samples from 300 to 700 K.



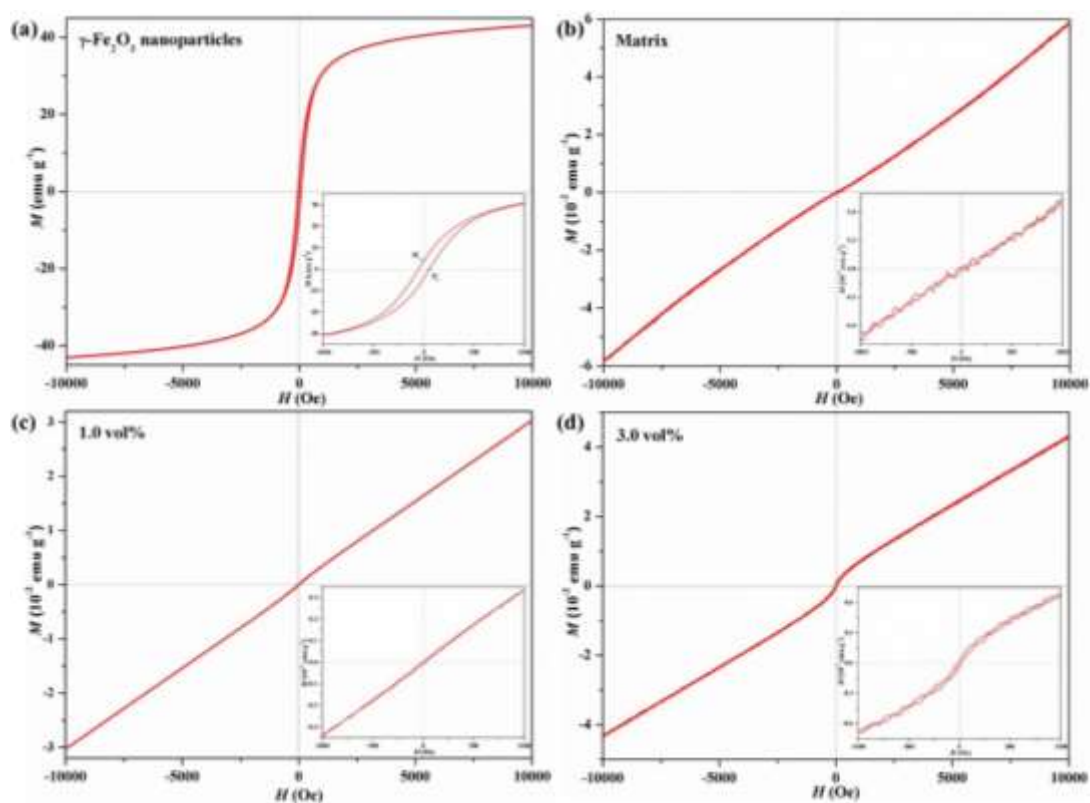


**Figure S8** Magnetization versus magnetic field ( $M$ - $H$ ) plots for (a) the  $\gamma$ - $\text{Fe}_2\text{O}_3$  NPs, (b) CNAS matrix, (c) CNAS-1.0% $\text{Fe}_2\text{O}_3$ , and (d) CNAS-3.0% $\text{Fe}_2\text{O}_3$  at room temperature.

The magnetic properties of the CNAS- $x\text{Fe}_2\text{O}_3$  were measured at room temperature and the results are shown in the Figure S8. The  $\gamma$ - $\text{Fe}_2\text{O}_3$  nanoparticles exhibit the strongest ferromagnetism as compared to the other three samples. The saturation magnetization ( $M_s$ ), remnant magnetization ( $M_r$ ), and coercivity ( $H_c$ ) of  $\gamma$ - $\text{Fe}_2\text{O}_3$  nanoparticles are about 31 emu/g, 3.5 emu/g and 62.5 Oe. The matrix reveals paramagnetism. Additionally, the CNAS-1.0% $\text{Fe}_2\text{O}_3$  and CNAS-3.0% $\text{Fe}_2\text{O}_3$  also exhibit paramagnetism, which may be due to the low content of magnetic  $\gamma$ - $\text{Fe}_2\text{O}_3$  nanoparticles. There is no magnetic transition from ferromagnetism to paramagnetism in CNAS- $x\text{Fe}_2\text{O}_3$  in the range 300-700 K, because the Curie temperature ( $T_C$ ) has been estimated as lying between 820 K and 986 K.<sup>1</sup>

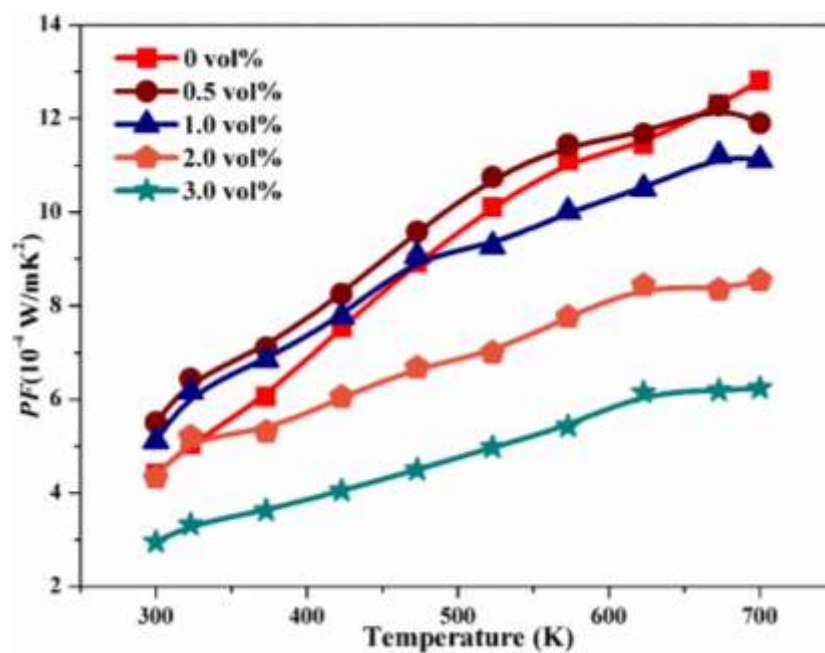


**Figure S9** Temperature dependence of the power factor for all samples.

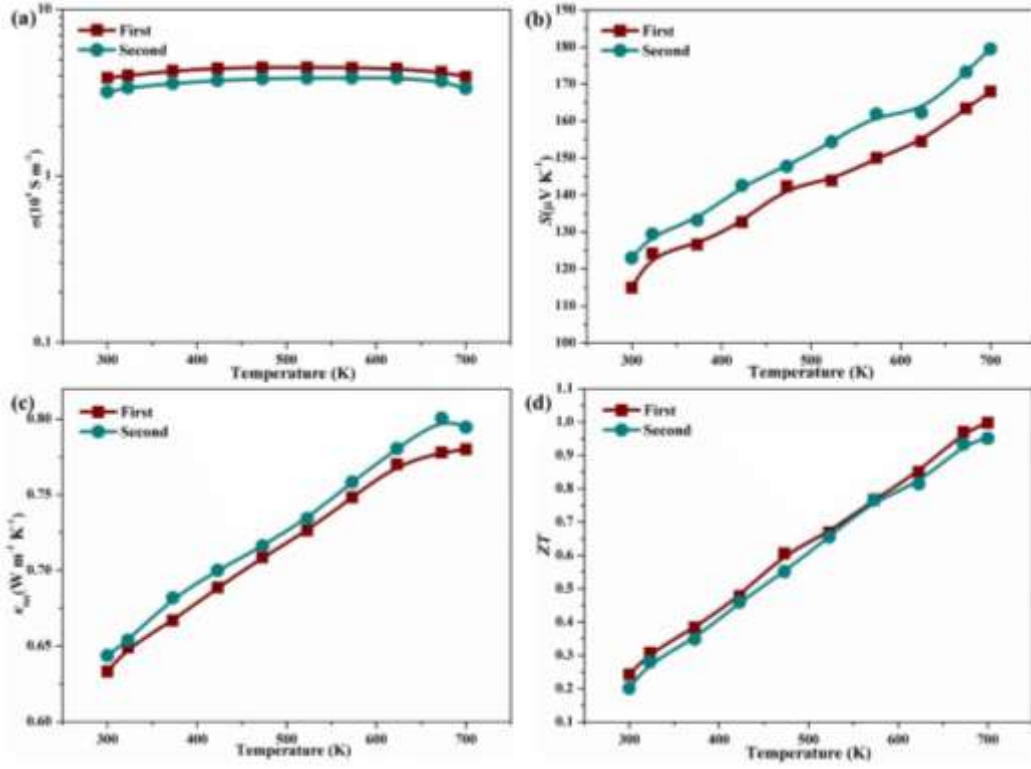


**Figure S10** Repeat measurement of (a) electrical resistivity, (b) Seebeck coefficient, (c) thermal conductivity, and (d) calculated ZT value of CNAS-1.0%Fe<sub>2</sub>O<sub>3</sub>.

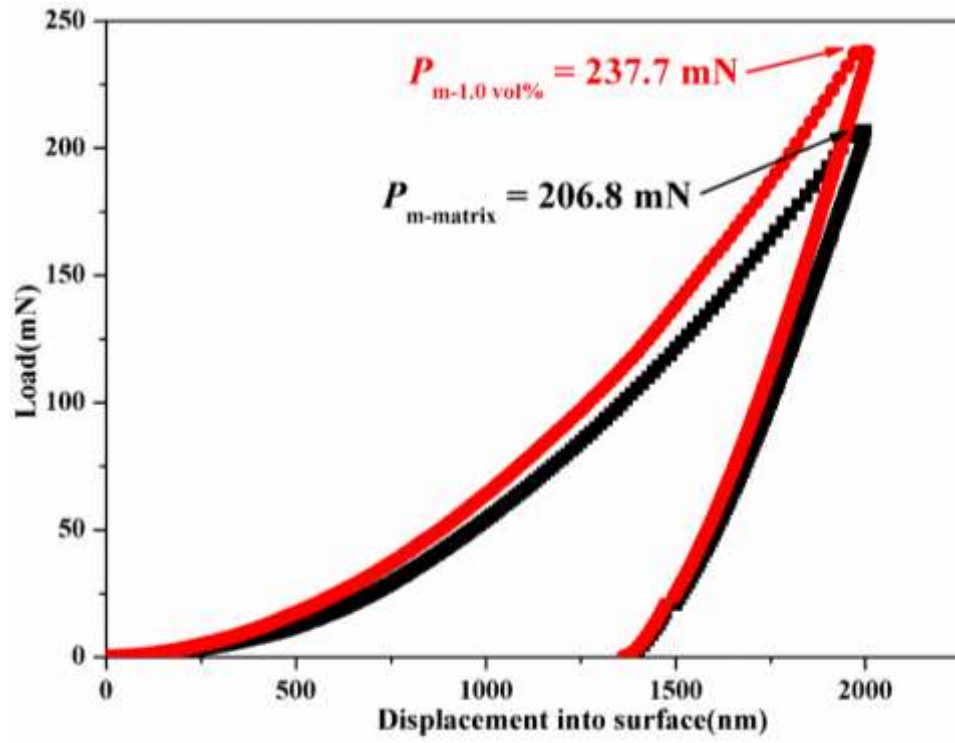


**Figure S11** Curves of load as a function of displacement into the surface and the maximum load ( $P_m$ ) is 206.8 and 237.7 mN for the matrix and CNAS-1.0%Fe<sub>2</sub>O<sub>3</sub> composite, respectively.

**Table S1 Density of different samples**

Samples	Theoretic density	0%	0.5%	1.0%	2.0%	3.0%
Density (g/cm <sup>3</sup> )	5.05	4.52	4.46	4.41	4.40	4.41

## REFERENCES

- (1) Cornell, R. M; Schwertmann, U. *The Iron Oxides: Structure, Properties, Reactions, Occurences and Uses*. Wiley-VCH, 2003; pp 128-130.